MFN= 007265
01 SID/SCD
02 5856
03 INPE-5856-PRE/1999
14 CEA
05 S
06 an
10 Chian, Abraham Chian Long
10 Rizzato, F.B
12 Coupling of electromagnetic filamentation instability
    and electrostatic Langmuir parametric instabilities in
    laser-plasma interactions
14 61-73
30 Journal Plasma Physics
31 51
32 Part 1
40 n
41 En
42 <E>
58 <P>
61 <PI>
64 <1994>
68 PPE
76 GEOFISICA ESPACIAL
93 The interaction of electromagnetic filamentation
    instability and eletrostatic Langmuir parametric
    instabilities (parametric decay instability and
    oscillating two-stream instability) driven by an intense
    laser in a plasma is examined. Near the critical layer
    of an underdense plasma where the incident laser
    frequency is close to the local plasma frequency,
    coupling of unstable electromagnetic and electrostatic
    modes may occur. The transition from purely
    electromagnetic and purely electrostatic instabilities
    to hybrid instabilities is analysed using the
    generalized Zakharov equations.
90 b
91 FDB-19960403
92 FDB-MLR

61

Coupling of electromagnetic filamentation instability and electrostatic Langmuir parametric instabilities in laser–plasma interactions

By A. C.-L. CHIAN† AND F. B. RIZZATO‡

Department of Applied Mathematics and Theoretical Physics, University of Cambridge, Silver Street, Cambridge, CB3 9EW, U.K.

The interaction of electromagnetic filamentation instability and electrostatic Langmuir parametric instabilities (parametric decay instability and oscillating two-stream instability) driven by an intense laser in a plasma is examined. Near the critical layer of an underdense plasma, where the incident laser frequency is close to the local plasma frequency, coupling of unstable electromagnetic and electrostatic modes may occur. The transition from purely electromagnetic and purely electrostatic instabilities to hybrid instabilities is analysed using the generalized Zakharov equations.

1. Introduction

In laser–plasma interaction plasma parametric instabilities play an important role. A rich variety of parametric processes can compete to determine the dynamics of the laser–plasma coupling (Chen 1974; Lashmore-Davies 1981; Bobin 1985; Kruer 1988).

The electromagnetic filamentation instability (FI), also known as the self-focusing instability, refers to the growth of zero-frequency density perturbations and the corresponding modulation of the incident laser light in the plane orthogonal to the propagation vector of the incident wave. The classical FI wave-vector kinematics is shown in figure 1 (Bingham & Lashmore-Davies 1976, 1979; Lashmore-Davies 1981). $(\omega_0, \mathbf{k}_0)$ is the electromagnetic pump wave, which interacts with low-frequency density perturbations $(\omega, \pm \mathbf{k})$ to induce a Stokes electromagnetic wave $(\omega_-, \mathbf{k}_0 - \mathbf{k})$ and an anti-Stokes electromagnetic wave $(\omega_+, \mathbf{k}_0 + \mathbf{k})$, where $\mathbf{k}$ is perpendicular to $\mathbf{k}_0$. The basic features of FI are that $\alpha \equiv k^2/k_0^2 \ll 1$ and there is pure growth $(\text{Re}\,(\omega) = 0)$; thus the Stokes and anti-Stokes electromagnetic waves have the same frequency as the pump wave. In laser-irradiated targets FI takes place throughout the underdense plasma, including the neighbourhood of the critical layer $n_{cr} = \omega_0^2 m_e \epsilon_0/e^2$, as shown in figure 2.

† Permanent address: National Institute for Space Research–INPE, P.O. Box 515, 12227-010 São José dos Campos–SP, Brazil.
‡ Present address: Instituto de Física, Universidade Federal do Rio Grande do Sul, Caixa Postal 15051, 91501-970 Porto Alegre–RS, Brazil.
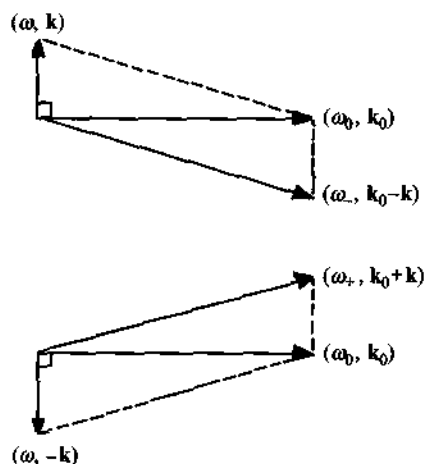
FIGURE 1. Geometry of wave-vector matching conditions for electromagnetic filamentation instability; $\alpha \equiv k^2/k_0^2 \ll 1$.
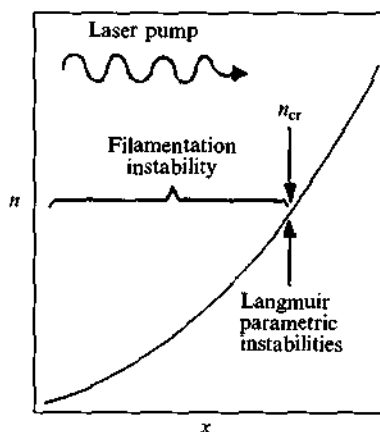

FIGURE 2. Typical density profile for laser-plasma interactions.

Near the critical layer, the laser pump can excite two types of electrostatic Langmuir parametric instabilities: parametric decay instability (PDI) and oscillating two-stream instability (OTSI) (Lashmore-Davies 1975, 1981), as shown in figures 2 and 3. In PDI (the top triplet of figure 3), an electromagnetic pump wave (ω_0, k_0) decays into a propagating ion-acoustic wave (ω, k) and a Stokes Langmuir wave $(\omega_-, k_0 - k)$; this instability is convective $(\text{Re}(\omega) \neq 0)$ and there is down-conversion $(\omega_- < \omega_0)$. In OTSI (both triplets of figure 3) the pump electromagnetic wave interacts with low-frequency density perturbations $(\omega, \pm k)$ to induce a Stokes Langmuir wave $(\omega_-, k_0 - k)$ and an anti-Stokes Langmuir wave $(\omega_+, k_0 + k)$. This instability is purely growing; thus the Stokes and anti-Stokes Langmuir waves have the same frequency as the pump wave. In general, for both PDI and OTSI, $\alpha \gg 1$. Note that in this paper Langmuir parametric instabilities refer to the electrostatic parametric processes driven by
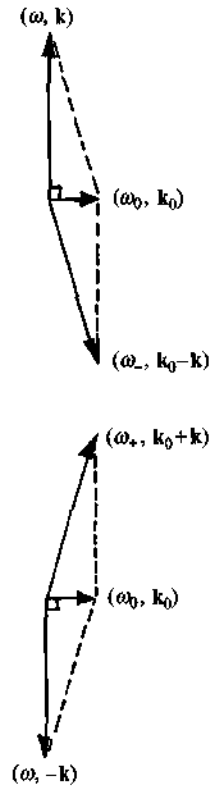
FIGURE 3. Geometry of wave-vector matching conditions for electrostatic Langmuir parametric instabilities; $\alpha \equiv k^2/k_0^2 \gg 1$.

an electromagnetic pump wave, in contrast to the usual Langmuir parametric instabilities driven by a Langmuir pump wave.

The objective of this paper is to study the coupling of FI, PDI and OTSI in the vicinity of n_{cr}, where the three parametric processes can compete with and influence each other. The filamentation instability and Langmuir parametric instabilities are purely electromagnetic and purely electrostatic respectively only if the intensity of the laser pump is relatively small. For strong laser pumps, hybrid (coupled electromagnetic–electrostatic) instabilities can be excited near the critical layer. It will be shown that, even for relatively weak laser pumps, coupling of unstable electromagnetic and electrostatic modes can take place for a certain range of plasma parameters. A proper understanding of this coupling is essential for obtaining the dynamical behaviour of laser–plasma interactions when the pump frequency ω_0 approaches the local plasma frequency $\omega_p = (n_0 e^2/m_e \epsilon_0)^{\frac{1}{2}}$.

The paper is structured as follows. In §2 the fundamental equations are discussed, and the nonlinear dispersion relation describing the coupling of FI, PDI and OTSI is derived. In §3 the nonlinear dispersion relation is analysed. In §4 our conclusions are presented.

2. Fundamental equations

The coupled wave equations describing the nonlinear interaction of high-frequency electromagnetic/electrostatic waves, close to the plasma frequency, with low-frequency density fluctuations are the generalized Zakharov equations (Kuznetsov 1974; Thornhill & ter Haar 1978; Akimoto 1988; Rizzato & Chian 1992; Li & Li 1993):

$$[\partial_t^2 + \omega_p^2 + c^2 \nabla \times \nabla \times - 3v_{\mathrm{th}}^2 \nabla(\nabla .)] \mathbf{E} = -\frac{\omega_p^2}{n_0} n \mathbf{E}, \tag{1}$$

$$(\partial_t^2 - c_S^2 \nabla^2) n = \frac{\epsilon_0}{2m_i} \nabla^2 \langle E^2 \rangle, \tag{2}$$

where $v_{\mathrm{th}} = (k_B T_e/m_e)^{\frac{1}{2}}$, $c_S = (k_B T_e/m_i)^{\frac{1}{2}}$, c is the velocity of light and the angular brackets denote the fast time average. The set of generalized Zakharov equations (1) and (2) was used by Akimoto (1988) and Rizzato & Chian (1992) to study the nonlinear generation of high-frequency electromagnetic and Langmuir waves by a Langmuir pump wave, via ponderomotive coupling with low-frequency density fluctuations. This formalism is a refinement of that in previous works by Chian & Alves (1988) and Chian (1991). In this paper we show that this set of equations can also describe the nonlinear coupling of electromagnetic filamentation instability and electrostatic Langmuir parametric instabilities, driven by an electromagnetic pump wave.

A high-frequency travelling electromagnetic pump wave $\mathbf{E}_0(\omega_0, \mathbf{k}_0)$, incident from left to right along the x axis with linear polarization along the y axis, interacts with low-frequency density fluctuations to emit secondary high-frequency waves $\delta\mathbf{E}(\omega_\mp, \mathbf{k}_\mp)$ with wave vectors lying in the (x, y) plane. The pump obeys the dispersion relation

$$\omega_0^2 = \omega_p^2 + c^2 k_0^2. \tag{3}$$

The induced high-frequency modes have frequency close to ω_0; hence

$$\delta\mathbf{E}_{hf} = \delta\mathbf{E}\, e^{-i\omega_0 t} + \text{c.c.}, \tag{4}$$

with $\omega_0|\delta\mathbf{E}| \gg |\partial_t \delta\mathbf{E}|$. The wave vector $\mathbf{k}$ of the low-frequency density fluctuations is assumed to be parallel to the y axis, with arbitrary magnitude. The characteristic wave-vector geometry is displayed in figure 4. It is evident from the figure that, depending on the ratio α, the secondary high-frequency modes may be predominantly electromagnetic $(\alpha \ll 1)$, electrostatic $(\alpha \gg 1)$ or hybrid $(\alpha = O(1))$.

Fourier analysis of (1) and (2) yields

$$[-2i\omega_p \partial_t - \delta_\omega - c^2 \mathbf{k} \times \mathbf{k} \times + 3v_{\mathrm{th}}^2 \mathbf{k}(\mathbf{k}.)] \delta\mathbf{E}(\mathbf{k}) = -\frac{\omega_p^2}{n_0} \int n(\mathbf{k}_1) \mathbf{E}_0(\mathbf{k}-\mathbf{k}_1)\, d\mathbf{k}_1, \tag{5}$$

$$d_S n = \frac{-k^2 \epsilon_0}{2m_i} \int [\mathbf{E}_0(\mathbf{k}-\mathbf{k}_1).\delta\mathbf{E}(-\mathbf{k}_1)^* + \mathbf{E}_0(\mathbf{k}_1-\mathbf{k})^*.\delta\mathbf{E}(\mathbf{k}_1)]\, d\mathbf{k}_1, \tag{6}$$

where $\delta_\omega \equiv \omega_0^2 - \omega_p^2$, $d_S \equiv \partial_t^2 + \omega_S^2$, $\omega_S^2 \equiv c_S^2 k^2$, and $n(\mathbf{k}) = n(-\mathbf{k})^*$ is the $\mathbf{k}$-Fourier component of the density fluctuations $n(\mathbf{r}, t)$ and $\delta\mathbf{E}(\mathbf{k})$ the $\mathbf{k}$-Fourier component of the high-frequency perturbed field $\delta\mathbf{E}(\mathbf{r}, t)$.
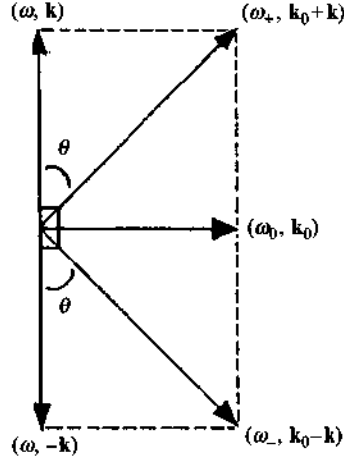
FIGURE 4. Geometry of wave-vector matching conditions for hybrid parametric instabilities; $\alpha \equiv k^2/k_0^2 = O(1)$.

Now we split the high-frequency field into its electromagnetic and electrostatic components:

$$\delta\mathbf{E} = \delta\mathbf{E}_T + \delta\mathbf{E}_L, \tag{7}$$

where $\delta\mathbf{E}_L$ ($\delta\mathbf{E}_T$) is parallel (perpendicular) to $\mathbf{k}$. By taking account that $\nabla \times \nabla \times \mathbf{E}_L = 0$ and $\nabla . \mathbf{E}_T = 0$, we obtain

$$\delta E_L(\mathbf{k}) = \frac{\omega_p^2}{2i\omega_p \, \partial_t + \delta_\omega - 3v_{\mathrm{th}}^2 k^2} \int \frac{n(\mathbf{k}_1)}{n_0} E_0(\mathbf{k} - \mathbf{k}_1) \cos\theta \, d\mathbf{k}_1, \tag{8}$$

$$\delta E_T(\mathbf{k}) = \frac{\omega_p^2}{2i\omega_p \, \partial_t + \delta_\omega - c^2 k^2} \int \frac{n(\mathbf{k}_1)}{n_0} E_0(\mathbf{k} - \mathbf{k}_1) \sin\theta \, d\mathbf{k}_1, \tag{9}$$

where θ is the angle between $\mathbf{k}$ and the wave vectors of the secondary high-frequency waves. If we write the pump electric field as

$$\mathbf{E}_0(\mathbf{k}) = \delta(k_x - k_0) \, \delta(k_y) \, \delta(k_z) E_0 \hat{\mathbf{y}},$$

it follows from (8) and (9) that

$$d_S \, n(\mathbf{k}) = [\cos^2\theta \, (\Lambda_L + \Lambda_L^*) + \sin^2\theta \, (\Lambda_T + \Lambda_T^*)] \, n(\mathbf{k}), \tag{10}$$

where

$$\Lambda_L \equiv \frac{-k^2 \epsilon_0 \, \omega_p^2 \, E_0^2}{2m_i n_0} \frac{1}{2i\omega_p \, \partial_t + \delta_\omega - 3v_{\mathrm{th}}^2 (\mathbf{k} + \mathbf{k}_0)^2}, \tag{11}$$

$$\Lambda_T \equiv \frac{-k^2 \epsilon_0 \, \omega_p^2 \, E_0^2}{2m_i n_0} \frac{1}{2i\omega_p \, \partial_t + \delta_\omega - c^2 (\mathbf{k} + \mathbf{k}_0)^2}. \tag{12}$$

If we assume harmonic solutions for the density fluctuations, the set of coupled wave equations (8)–(10) yields the nonlinear dispersion relation

$$\omega^2 - \omega_S^2 = \omega_S^2 \, \omega_p \, W\left(\frac{\delta_L \cos^2\theta}{\omega^2 - \delta_L^2} + \frac{\delta_T \sin^2\theta}{\omega^2 - \delta_T^2}\right), \tag{13}$$

with
$$\delta_L \equiv \frac{\omega_L^2 - \omega_0^2}{2\omega_p} = \eta\left(\epsilon\frac{k_0^2 + k^2}{k_0^2} - 1\right) \approx \omega_L - \omega_0, \tag{14}$$

$$\delta_T \equiv \frac{\omega_T^2 - \omega_0^2}{2\omega_p} = \eta\frac{k^2}{k_0^2} \approx \omega_T - \omega_0, \tag{15}$$

$$W = \frac{\epsilon_0 E_0^2}{8n_0 k_B T_e}, \tag{16}$$

$$\eta = \frac{c^2 k_0^2}{2\omega_p}, \tag{17}$$

$$\epsilon = \frac{v_{th}^2}{c^2} = \frac{k_B T_e}{m_e c^2}, \tag{18}$$

where ω_L is the linear (unperturbed) frequency of the induced Langmuir waves, ω_T is the linear frequency of the induced electromagnetic modes, δ_L is an electrostatic detuning factor that measures the linear frequency shift of the induced Langmuir waves, δ_T is an electromagnetic detuning factor that measures the linear frequency shift of the induced electromagnetic waves, and W measures the pump intensity.

If we now normalize frequencies as $\omega \to \omega/\eta$, and redefine the pump intensity as $W \to \hat{W} = (\omega_p/\eta)\, W$, we can finally write the nonlinear dispersion relation in a non-dimensional and convenient form

$$\omega^2 - \beta\alpha = \beta\hat{W}\frac{\alpha^2}{1+\alpha}\left[\frac{\epsilon(1+\alpha)-1}{\omega^2 - (\epsilon(1+\alpha)-1)^2} + \frac{1}{\omega^2 - \alpha^2}\right], \tag{19}$$

where we have further introduced $\beta \equiv c_S^2 k_0^2/\eta^2$ (recall that $\alpha \equiv k^2/k_0^2$). The relation (19) will hereinafter be referred to as the hybrid dispersion relation. In deriving (13) and (19), the following modes have been taken into consideration in the interaction (see figure 4): laser pump wave $E_0(\omega_0, k_0)$, low-frequency density waves $n(\omega, \pm k)$, Stokes and anti-Stokes electromagnetic waves $\delta E_T(\omega_\mp, k_0 \mp k)$, and Stokes and anti-Stokes Langmuir waves $\delta E_L(\omega_\mp, k_0 \mp k)$.

3. Analysis of the nonlinear dispersion relation

Before analyzing the hybrid instabilities involving the coupling of unstable electromagnetic and electrostatic modes, let us treat some limiting cases where the instabilities are decoupled into purely electromagnetic or electrostatic modes.

3.1. Purely electromagnetic case ($\alpha \ll 1$)

The purely electromagnetic case arises when the wave vectors of the secondary high-frequency wave are almost parallel to the x axis, which implies $\alpha \ll 1$ (see figure 1). In this case we can discard the electrostatic contribution to the hybrid dispersion relation; (19) then reduces to

$$\omega^2 - \beta\alpha = \frac{\beta\alpha^2\hat{W}}{\omega^2 - \alpha^2}. \tag{20}$$

Now noting that secondary electromagnetic waves have wavenumbers larger than k_0 (i.e. $|k_0 \mp k| > |k_0|$), and consequently larger unperturbed frequencies than ω_0 as well (i.e. $\omega_\mp^2 (k_0 \mp k) = \omega_p^2 + c^2(k_0^2 + k^2) > \omega_0^2$), we conclude that the interaction process cannot be of the decay type. Then, on writing $\omega = i\Gamma$ (Γ real) to search for purely growing modes, we have from (20)

$$\Gamma^2 + \beta\alpha = \frac{\beta\alpha^2 \hat{W}}{\alpha^2 + \Gamma^2}. \tag{21}$$

Equation (21) yields a threshold condition ($\Gamma = 0$), $\hat{W} = \alpha$, owing to finite detuning, and has a real root for

$$\alpha < \hat{W}, \tag{22}$$

which shows that the instability is purely electromagnetic (i.e. $\alpha \ll 1$) only when $\hat{W} \ll 1$, namely the weak pump regime. This case corresponds to the electromagnetic filamentation instability, FI (Bingham & Lashmore-Davies 1976, 1979; Lashmore-Davies 1981).

3.2. *Purely electrostatic case* ($\alpha \gg 1$)

In the region of large α ($\alpha \gg 1$) the wave vectors of the secondary high-frequency waves are almost parallel to the y axis (see figure 3). In this case the electromagnetic contribution to the hybrid dispersion relation may be discarded. Hence (19) reduces to

$$\omega^2 - \beta\alpha = \beta\alpha\hat{W}\left[\frac{\epsilon\alpha - 1}{\omega^2 - (\epsilon\alpha - 1)^2}\right]. \tag{23}$$

The resulting electrostatic system turns out to be more complex than the purely electromagnetic case because we can now identify two possible situations as the factor α is varied. Indeed it can be verified that there is a critical value α_{cr} such that for $\alpha > \alpha_{cr}$ the unperturbed frequency of the secondary Langmuir wave is larger than ω_0, while for $\alpha < \alpha_{cr}$ it is smaller. This critical quantity α_{cr} may be evaluated from the condition $\delta_L = 0 \Rightarrow (\epsilon\alpha_{cr} - 1)^2 = 0$, which yields

$$\alpha_{cr} \approx \frac{1}{\epsilon}, \tag{24}$$

a quantity much greater than unity for plasmas of non-relativistic temperatures. If $\alpha > \alpha_{cr}$ the interaction dynamics is similar to the purely electromagnetic case of §3.1. There is no possibility of decay in this case, and what we have is a purely growing low-frequency density mode whose unstable αs are located in the range

$$\alpha_{cr} < \alpha < \frac{\hat{W} + 1}{\epsilon}. \tag{25}$$

We can see that the range may be either narrow or wide, depending on the pump intensity. This case corresponds to the Langmuir oscillating two-stream instability, OTSI (Lashmore-Davies 1975, 1981).

When $\alpha < \alpha_{cr}$, the instability reduces to the Langmuir parametric decay instability, PDI (Lashmore-Davies 1975, 1981). In the weak pump regime the
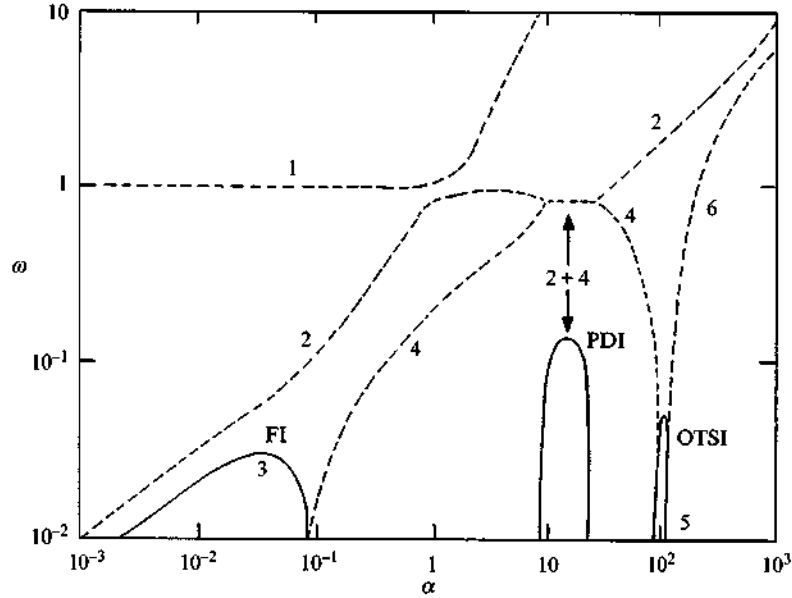
FIGURE 5. Overview of the uncoupled instabilities for $\hat{W} = 0.1$ and $\beta = 0.05$: ———, imaginary parts of the frequency of the unstable modes; ————, real parts; FI, electromagnetic filamentation instability; PDI, electrostatic parametric decay instability; OTSI, electrostatic oscillating two-stream instability.

peak of the instability is located at the resonance defined by $(\epsilon\alpha_{peak} - 1)^2 - \beta\alpha_{peak} = 0$, corresponding to the acoustic wave (left-hand side of (23)) and the Langmuir wave (the denominator of the right-hand side of (23)) being driven at their natural frequencies, which can be seen to yield large values of α_{peak} only when $\beta \ll 1$, which is something that can always occur for large enough values of k_0, or specifically when

$$\frac{c_S^2}{c^2}\frac{\omega_p^2}{c^2 k_0^2} \ll 1.$$

If, on the other hand, β is too large (i.e. $\beta = O(1)$) then the instability would have its peak located at too small values of α_{peak} for the electrostatic-electromagnetic decoupling to be operative. This particular case has not been analysed before, and it should be emphasized that here hybrid modes are generated even in the weak-pump regime. The instability width of these unstable modes can be estimated to be proportional to $\hat{W}^{\frac{1}{4}}$ for the weak-pump regime. The range is expected to grow as $\hat{W}$ gets larger. This observation allows us to conclude that the conditions for the parametric decay instability to be purely electrostatic (or entirely situated at large values of α) are $\beta \ll 1$ and $\hat{W} \ll 1$.

In figure 5 we plot the frequency of the various unstable modes in the weak pump regime for $\beta \ll 1$, taking $\hat{W} = 0.05$, $\beta = 0.1$ and $\epsilon = 0.01$. The three basic unstable modes are clearly seen: mode {3} is the purely growing electromagnetic filamentation instability (FI); mode {2 + 4} is the electrostatic parametric decay instability (PDI), which appears as the result of the fusion of modes {2} and {4}; and mode {5} is the purely growing electrostatic oscillating two-stream
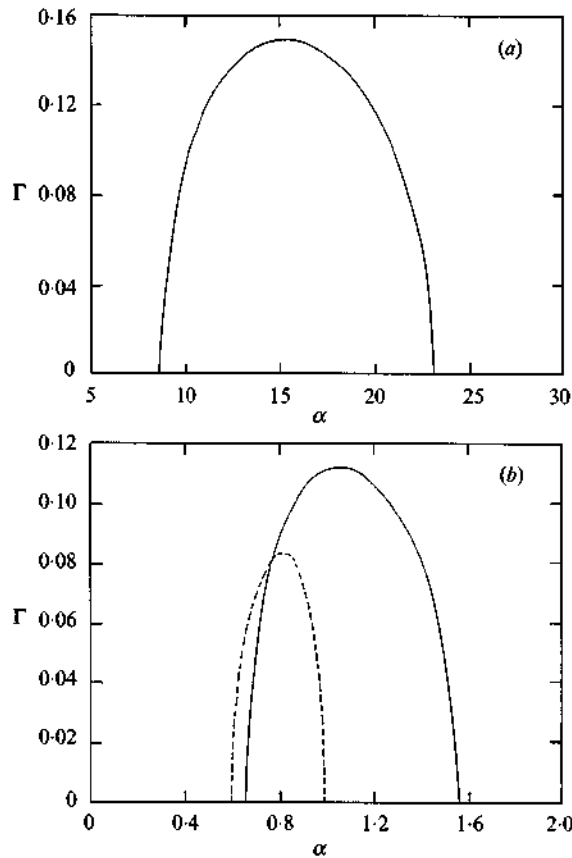
FIGURE 6. Growth rates for the parametric decay instability for $\hat{W} = 0\cdot1$ and $\beta = 0\cdot05$ (*a*) and $\beta = 1\cdot0$ (*b*): ----, uncoupled dispersion relation; ——, hybrid dispersion relation.

instability (OTSI). From the figure we can see that the various unstable modes occur in quite distinct regions along the α axis.

As a general rule, we can conclude that the necessary conditions to decouple electromagnetic modes from electrostatic ones are $\hat{W} \ll 1$ and $\beta \ll 1$. If these conditions are not satisfied then mode-mixing will occur in some regions of α space. Let us now proceed with our investigation to determine the basic characteristics of these hybrid modes.

3.3. *Hybrid case* $(\alpha = O(1))$

First let us consider the behaviour of the PDI mode in the weak-pump regime. For small β (i.e. $\beta \ll 1$) this mode is nearly electrostatic. For large β (i.e. $\beta \gg 1$) the mode becomes hybrid. In figure 6 we plot the growth rate as a function of α for $\hat{W} = 0\cdot1$ and $\beta = 0\cdot05$ (*a*) and $\beta = 1\cdot0$ (*b*). For small β the hybrid and uncoupled dispersion relations yield practically the same growth rate, as shown in figure 6(*a*), where the full and dotted lines representing them are indistinguishable. For large values of β the purely electrostatic description of PDI becomes inaccurate, since the PDI mode then turns into a hybrid mode, as evidenced in figure 6(*b*).

The other factor that may couple the various instabilities is the pump intensity $\hat{W}$. Let us begin to study its effect by examining the behaviour of purely growing unstable modes. We write $\omega = i\Gamma$ in (19) to obtain

$$\Gamma^2 + \beta\alpha = \beta W \frac{\alpha^2}{1+\alpha}\left[\frac{\epsilon(1+\alpha)-1}{(\epsilon(1+\alpha)-1)^2+\Gamma^2} + \frac{1}{\alpha^2+\Gamma^2}\right]. \tag{26}$$

If α is much smaller than unity, we recover the case of electromagnetic filamentation instability as before. However, for larger α the situation may change. The effect of the electrostatic term in (26) is to cause the function defined by the right-hand side to curve downwards on approaching $\Gamma = 0$. It may happen that owing to this curvature, two mutual intersections of the right- and left-hand sides, $R(\Gamma^2)$ and $L(\Gamma^2)$, become possible, similarly to what can be observed in figure 6 of Rizzato & Chian (1992). The existence condition for this situation is closely related to the intensity of the pump power. Indeed, noting that for small values of Γ, $R(\Gamma^2)$ decreases monotonically with α and $|dR(\Gamma^2)/d\alpha|$ decreases with Γ^2, one can readily derive the critical existence condition for the simultaneous presence of two roots as

$$L(\Gamma^2)|_{\Gamma^2=0} = R(\Gamma^2)|_{\Gamma^2=0},$$

$$\frac{dR(\Gamma^2)}{d\Gamma^2}\bigg|_{\Gamma^2=0} = 0,$$

which yields the critical values

$$\alpha_C \approx 1 - \tfrac{3}{2}\epsilon, \tag{27}$$

$$\hat{W}_C \approx \frac{2}{\epsilon} \gg 1. \tag{28}$$

These critical values are to be interpreted as yielding α_C and $\hat{W}_C$ such that if $\hat{W}$ is larger than $\hat{W}_C$ then there will be some value of α, larger than α_C, for which the two roots simultaneously appear. The larger of the two roots is an extension of the one corresponding to the electromagnetic filamentation mode already present for $\alpha \ll 1$, but the smaller represents a new unstable mode that does not occur either for smaller α or for smaller $\hat{W}$. We should point out that this second purely growing mode is always hybrid because it appears only for $\alpha \geqslant \alpha_C = O(1)$.

The transition from uncoupled modes to hybrid modes as the pump intensity increases is illustrated in figure 7. For small $\hat{W}$, FI and PDI remain essentially purely electromagnetic and electrostatic respectively. As the pump amplitude gets larger, the unstable range of these modes in α space also gets larger; moreover, the FI and PDI modes turn into hybrid modes and eventually merge with each other. Note that the OTSI mode, which occurs for large α, does not appear in figure 7 because of the scale adopted. Our numerical solutions indicate that OTSI remains essentially uncoupled even for large pump intensities.

In figure 8 an overview of the strong pump instabilities is presented for $\beta = 1\cdot0$, $\epsilon = 0\cdot01$ and $\hat{W} = 2 \times 10^3$, which is larger than the respective critical intensity $\hat{W}_C = 2 \times 10^2$. In the region of very small α it is possible to see the purely growing FI mode {3}, while for α closer to $\alpha_C = O(1)$ the second purely growing {4} mode does appear. These two modes meets at a terminal point J,
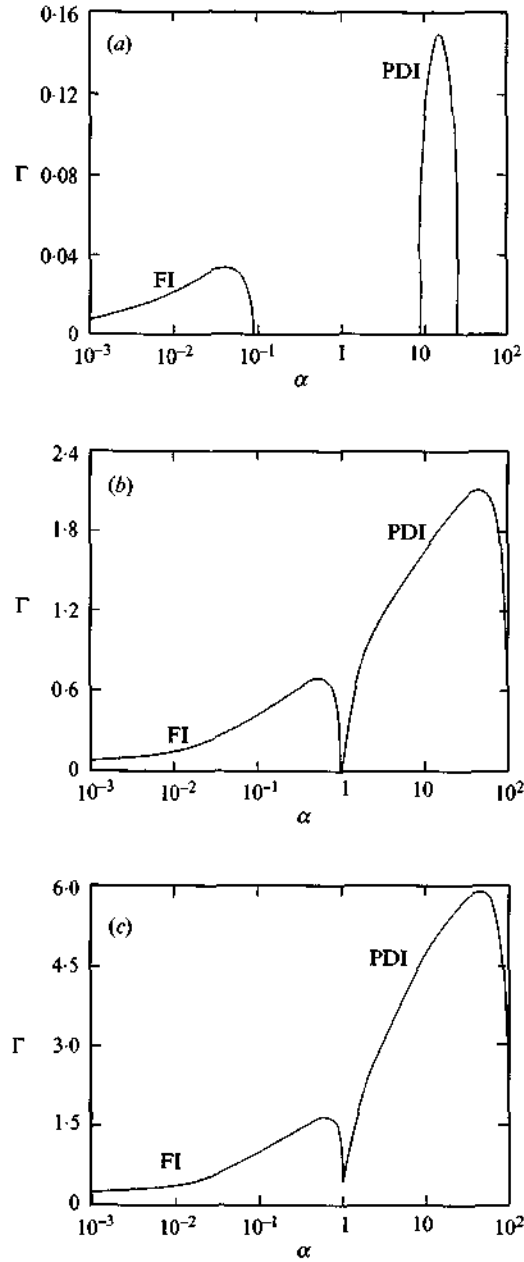
FIGURE 7. Transition from purely electromagnetic and electrostatic modes to hybrid modes for $\epsilon = 0.01$, $\beta = 0.05$ and $\hat{W} = 0.1$ (a), $\hat{W} = 100$ (b) and $\hat{W} = 2 \times 10^3$ (c).

where the instability is converted into PDI {5}. The parametric decay instability extends up to α_{cr}, where it vanishes. Above α_{cr} the only remaining unstable mode is OTSI {6}. Besides these modes, a new convective instability {1+2} is present for values of α that are not too large. It can be shown numerically that this instability is always hybrid. It appears only in the strong-
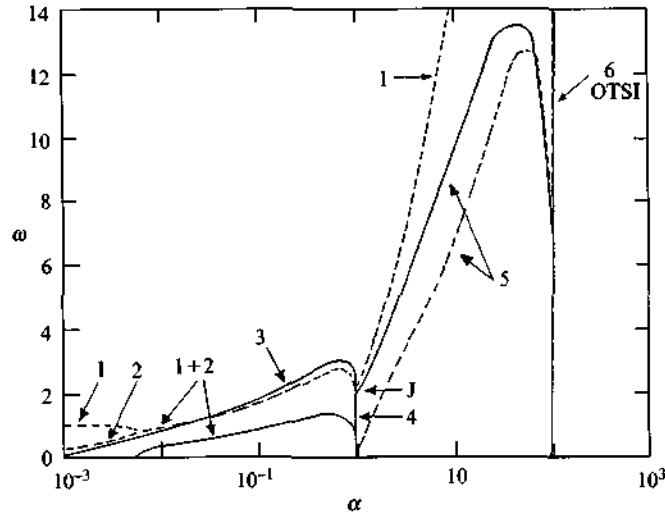
FIGURE 8. Overview of the hybrid instabilities for $\hat{W} = 2 \times 10^3$, and $\beta = 1.0$: ———,
imaginary parts of the frequencies of the unstable modes; – – – –, real parts.

pump regime; the same applies to mode {4} and point J. For smaller $\hat{W}$ the point
J is absent, and there is no direct connection between PDI and the purely
growing unstable modes {3} and {4}.

4. Final remarks

In this paper we have analysed the nonlinear coupling of electromagnetic
filamentation instability and electrostatic Langmuir parametric instabilities
induced by a powerful laser in the vicinity of the critical layer of an underdense
plasma, using the generalized Zakharov equations.

Assuming the wave vector of the low-frequency density fluctuations to be
perpendicular to the wave vector of the laser pump, we have identified a great
variety of unstable modes as the normalized wave vector α of the low-frequency
density fluctuations is varied. By classifying the unstable modes as pure or
hybrid, we have shown that when the intensity of the pump wave $\hat{W}$ and the
factor β are both much smaller than unity, all the unstable modes are pure,
either of the electromagnetic or electrostatic type. In this weak-pump regime
the unstable modes have been shown to be electromagnetic and purely growing
for $\alpha \ll 1$ (FI), electrostatic and convective for $1 \ll \alpha < \alpha_{cr}$ (PDI), and
electrostatic and purely growing for $\alpha > \alpha_{cr} \gg 1$ (OTSI).

In the case of a weak pump with larger β such that $\beta = O(1)$, we have shown
that the formerly purely electrostatic parametric decay instability (PDI) is
converted into a hybrid instability involving both electrostatic and electro-
magnetic effects.

Finally, in the strong-pump regime we have shown that, in addition to the
widening of the unstable range in α space of the previously identified modes,
some new instabilities may be excited. In this regard, we have examined the
appearance of new instabilities for $\alpha = O(1)$, of both the purely growing and
convective types. In particular, we have shown that, for strong laser intensities,

filamentation and Langmuir parametric decay instabilities can turn into hybrid instabilities, resulting in nonlinear coupling between these two instabilities near the critical layer.

REFERENCES

AKIMOTO, K. 1988 *Phys. Fluids* **31**, 538.

BINGHAM, R. & LASHMORE-DAVIES, C. N. 1976 *Nucl. Fusion* **16**, 67.

BINGHAM, R. & LASHMORE-DAVIES, C. N. 1979 *Plasma Phys.* **21**, 433.

BOBIN, J. L. 1985 *Phys. Rep.* **122**, 173.

CHEN, F. F. 1974 *Laser Interaction and Related Plasma Phenomena*, vol. 3A (ed. H. J. Schwarz & H. Hora), p. 291. Plenum.

CHIAN, A. C.-L. 1991 *Planet. Space Sci.* **39**, 1217.

CHIAN, A. C.-L. & ALVES, M. V. 1988 *Astrophys. J.* **330**, L77.

KRUER, W. L. 1988 *The Physics of Laser Plasma Interactions*. Addison-Wesley.

KUZNETSOV, E. A. 1975 *Soviet Phys. JETP* **39**, 1003.

LASHMORE-DAVIES, C. N. 1975 *Plasma Phys.* **17**, 281.

LASHMORE-DAVIES, C. N. 1981 *Plasma Physics and Nuclear Fusion Research* (ed. R. D. Gill), p. 319. Academic.

LI, L. H. & LI, X. Q. 1993 *Phys. Fluids* B **5**, 3819.

RIZZATO, F. B. & CHIAN, A. C.-L. 1992 *J. Plasma Phys.* **48**, 71.

THORNHILL, S. G. & TER HAAR, D. 1978 *Phys. Rep.* **43**, 43.